LAWRENCE
LIVERMORE
NATIONAL
LABORATORY

LLNL-JRNL-539131

Determination of the "NiOOH" charge and discharge mechanisms at ideal activity.

M. D. Merrill, M. A. Worsley, M. Stadermann

March 19, 2012

Journal of Electroanalytical Chemistry

Disclaimer

This document was prepared as an account of work sponsored by an agency of the United States government. Neither the United States government nor Lawrence Livermore National Security, LLC, nor any of their employees makes any warranty, expressed or implied, or assumes any legal liability or responsibility for the accuracy, completeness, or usefulness of any information, apparatus, product, or process disclosed, or represents that its use would not infringe privately owned rights. Reference herein to any specific commercial product, process, or service by trade name, trademark, manufacturer, or otherwise does not necessarily constitute or imply its endorsement, recommendation, or favoring by the United States government or Lawrence Livermore National Security, LLC. The views and opinions of authors expressed herein do not necessarily state or reflect those of the United States government or Lawrence Livermore National Security, LLC, and shall not be used for advertising or product endorsement purposes.

Determination of the "NiOOH" charge and discharge mechanisms at ideal activity.

Matthew Merrill, Marcus Worsley, and Michael Stadermann.

Abstract

The cathodic deposition of "NiOOH" from nickel nitrate solutions onto graphite produced active materials capable of being charged up to 1.84 +/- 0.02 e^- per Ni on and subsequently delivering 1.58 +/- 0.02 e^- per Ni ion or 462 mAhr/g. The graphite substrate caused an unusual deposition mechanism and yielded the highly active "NiOOH" due to an overlap of nitrate reduction, hydrogen evolution, and metallic Ni deposition reactions. The ability of the "NiOOH" to deliver an approximately ideal charge and discharge facilitated a coulometric and thermodynamic analysis through which the previously poorly resolved charge/discharge mechanisms were determined from known enthalpies of formation. The mechanisms were in accordance with the pH, potential dependence, charge quantities, hysteresis, and fluoride ion partial inhibition of the charge and discharge curves as well as Corrigan's spectroscopic results. The results indicated that there was little change in Ni ion valence and that the charge predominantly resulted from oxygen redox activity.

Introduction

Nickel-zinc batteries are promising for high power density energy storage applications. While Li-ion batteries have greater energy densities, Ni-Zn batteries are attractive in high power applications because their active materials have fast kinetics and electrolytes have higher conductivities [1]. High power battery performances can be further improved through the electrode's architecture, where porosity can be optimized for the mass transport of reactant ions though the electrolyte and for thinner active layer thicknesses. Thinner nickel oxide hydroxide (NiOOH) active layers distributed over more porous current collectors would have lower resistances for transporting H^+ though the material during

charge/discharge as well as minimize the electrical conductivity problems of the discharged $Ni(OH)_2$ state. Recent developments in architecture control of highly porous, electrically conductive, and light weight graphitic carbon monoliths makes these materials interesting for application as current collectors in Ni-Zn batteries [2-4]. We are therefore interested in the development of uniform, nano-scale "NiOOH" coatings which can be applied within sub-micron sized pores of graphitic carbon current collectors. While ultimately intended for application to highly porous graphitic carbon current collectors, the goal of this work is to characterize the deposition process and deposited material on a flat surface of highly oriented pyrolytic graphite (HOPG) in order to evaluate its feasibility for deposition into the more complex, porous graphitic current collector.

NiOOH active materials are primarily made through either chemical or electrochemical precipitation [1, 5]. Whether for use in nickel-zinc, nickel-metal hydride, nickel-hydrogen, or nickel-cadmium batteries, industry conventionally synthesizes chemically precipitated NiOOH particles and mechanically impregnates porous Ni foams or meshes with the particles. Industry's NiOOH electrodes demonstrate excellent stabilities of 1,000 – 10,000 cycles and moderate activities of 0.4 e^- per Ni atom or 115 mAhr/g $Ni(OH)_2$ [1, 5]. The specific energy of the NiOOH electrode is limiting for the Ni-Zn battery as Zn activity is ~900 mAhr/g. Reactions (1) and (2) describe the half-cell reactions of this battery type:

$$NiOOH + e^- + H^+ \leftrightarrow Ni(OH)_2 \quad (1)$$

$$Zn + 2 \cdot H_2O \leftrightarrow Zn(OH)_2 + 2 \cdot e^- + 2 \cdot H^+ \quad (2)$$

Using industry's methods of mechanically impregnating sub-micron pores with relatively large NiOOH particles is not a practical means of forming uniform, active layers of sub-micron thickness, particularly if lighter weight but more brittle carbon current collectors are used instead of metal Ni meshes. An attractive alternative is to use either anodic or cathodic electrodeposition methods for synthesizing uniform, nano-scale NiOOH films within a porous battery electrode current collector. The anodic deposition of nano-scale NiOOH films in micron-sized pores has been recently demonstrated [6]

however it remains unclear whether cathodic deposition methods remain a viable alternative, particularly when the storage of > 1 e^- per Ni might be possible.

The storage of > 1 e^- per Ni ion may be possible because the reaction indicated by (1) represents the simplification of a poorly understood mechanism [1, 5]. The active material produced through the oxidation of $Ni(OH)_2$ will be referred to as "NiOOH" for the sake of expediency and not specifically to the $Ni_2O_3(H_2O)$ state, where the Ni valence is 3.00+ . The "NiOOH" active material is known to be oxidizable to a state comparable to $Ni^{3.5+ - 4+}$ although the included redox activity of oxygen has been well-speculated [7-9]. Corrigan has proposed the following mechanism (3) which indicates a maximum charge of $Ni^{3.67+}$.

$$Ni_3(OH)_6(H_2O)_2 + K^+ + 6 \cdot OH^- \leftrightarrow K(NiO_2)_3(H_2O)_2 + 5 \cdot e^- + 6 \cdot H_2O \qquad (3)$$

Corrigan *et al* were able to spectroscopically determine that only one adsorption band, which is both strong and broad, changes with charge. The change of only the one adsorption band, whose intensity was proportional to the state of charge, indicated a single mixed-valent phase change [7]. The spectra were approximately independent of electrolyte cation composition (K^+, Na^+, or Li^+), were not consistent with the presence of hydroxide radicals, and the absence of Ni-OH bonds in the fully charged state indicated that all of the material's H^+s were discharged when fully oxidized [7-9]. Corrigan's thorough evaluation of the active nickel material with multiple spectroscopic techniques was, however, not accompanied by a thermodynamic analysis of the charge/discharge kinetics.

Cathodic deposition methods of "NiOOH" typically utilize the pH gradient generated by the electrochemical oxidation of NO_3^- through (4) to chemically precipitate $Ni(OH)_2$ according to (5), which is subsequently oxidized to "NiOOH" upon the first charge [7, 10, 11]. The further oxidation of NO_2^- to either N_2 or NH_4^+ can electrochemically generate a pH gradient with a 4 OH^- per 3 e^- ratio [12]. A pH gradient can alternatively be electrochemically generated by the reduction of water to form molecular hydrogen according to reaction (6). Note that the $Ni(OH)_2$ deposit chemically precipitated from the pH

gradient is an insulator which does not become conductive until oxidation by the initial charge and that reactions (4) and (6) are being catalyzed by the current collector [10]. The insulation of the current collector by $Ni(OH)_2$ means that the deposition process becomes self-limiting unless the $Ni(OH)_2$ remains porous enough to sustain diffusion of H_2O and NO_3^- reactant and OH^- product through the deposit. Unlike Pt or Ni alloys, the hydrogen evolution reaction (6) experimentally occurs at approximately the same potential as the nitrate oxidation (4) on graphitic carbon despite the difference in equilibrium potentials [11, 13]. The effect of the current collector's composition further complicates the deposition because the reduction of Ni^{2+} to the metallic state Ni^0 according to (7) is also a possible reaction pathway [12]. Water is not electrochemically stable on Ni at moderate potentials and will oxidize Ni^0 to $Ni(OH)_2$ through (8) [14]. Methods which take advantage of combining reactions (7) and (8) involve repetitively changing the applied potential from an extremely negative value to deposit Ni^0 by (6) and then shifting the potential to a more neutral value for (7) with cyclic voltammetry or pulse techniques [15]. While an example in the literature does exist where a uniformly thin and compact $Ni(OH)_2$ was cathodically deposited onto carbon nanotubes using extremely large pulse current densities, a value of 900 F/g over a 0.5 V window only corresponds to an activity of 0.43 e^- per Ni ion or 125 mAhr/g [16]. It is reported here how the deposition mechanisms can be managed to produce "NiOOH" capable of 1.58 e^- per Ni or 462 mAhr/g.

Table 1. Equations (4) – (8): The $Ni(OH)_2$ deposition mechanisms [12].

$$NO_3^- + 2\cdot e^- + H_2O \leftrightarrow NO_2^- + 2\cdot OH^- \quad (4)$$

$$E_0(4) = 0.835 - 0.0592\cdot pH + 0.0296\cdot \log\left(\left[NO_3^-\right]/\left[NO_2^-\right]\right)$$

$$Ni^{2+} + 2\cdot OH^- \leftrightarrow Ni(OH)_2 \quad (5)$$

$$\log\left(Ni^{2+}\right) = 12.18 - 2\cdot pH$$

$$2\cdot H_2O \leftrightarrow H_2 + 2\cdot OH^- \quad (6)$$

$$E_0(6) = 1.228 - 0.0592\cdot pH + 0.0592\cdot \log\left(\left[H^-\right]/\left[H_2\right]\right)$$

$$Ni^{2+} + 2\cdot e^- \leftrightarrow Ni \quad (7)$$

$$E_0(7) = -0.250 + 0.0296 \cdot \log([Ni^{2+}])$$

$$Ni + H_2O \leftrightarrow Ni(OH)_2 + 2 \cdot e^- \quad (8)$$

$$E_0(8) = 0.110 - 0.0596 \cdot pH$$

Methods

Electrochemical experiments were performed in a Teflon electrochemical cell. A Teflon face plate and corrosion-resistant silicone gasket (McMaster-Carr) exposed a circular, 1 cm diameter (0.785 cm^2) working electrode surface of highly oriented pyrolytic graphite (HOPG, ZYH grade, Bruker AFM Probes) on the bottom of the chamber. Used HOPG surfaces were removed with (Scotch) tape to expose a new, clean surface. A coiled 30 ga platinum wire (Hauser & Miller) counter electrode and double junction, SCE reference electrode (Radiometer Analytical) were inserted into the cell chamber from the top. The electrochemical experiments were performed with a Biologic VSP electrochemical workstation. Masses of the $Ni(OH)_2$ active material were determined by dissolving samples in 2 ml of 10 % w/v nitric acid under sonication for 15 minutes and then analyzing the Ni through inductively coupled plasma mass spectrometry (ICP-MS) (Thermo_Scientific X series 2). Scanning electron microscopy (SEM) and energy-dispersive X-ray spectroscopy (EDX) characterization were performed on a JEOL 7401-F at 5-10 keV (20mA) in secondary electron imaging mode with a working distance of 2-8 mm.

Results and discussion

The potentials of the nitrate reduction reaction (4) and the metallic nickel deposition reaction (7) on graphitic carbon were difficult to resolve because they occurred at the onset of hydrogen evolution (6). All of the reactions were expected to be interdependent. For example, the deposition of Ni^0 affects hydrogen evolution while the reduction of NO_3^- by H_2 is thought to suppress hydrogen bubble formation [10]. Small voltammetric peaks or shoulders of peaks occurred at the smallest current densities (Figure 1) and likely corresponded to metallic deposition because it was observed for $Ni(NO_3)_2$,

$NiCl_2$, and $Ni(ClO_4)_2$ electrolytes. The initial charges in 1 M KOH of deposits formed at -1 mA/cm^2 from $NiCl_2$ and $Ni(ClO_4)_2$ electrolytes initiated near -0.3 V vs SHE, which corresponded closely with the potential of metallic nickel oxidation (6). In addition to containing 5 – 10 % Ni^0, the deposits from $NiCl_2$ and $Ni(ClO_4)_2$ had significant black coloration which indicated the presence of anhydrous NiO [12]. The deposits from $Ni(NO_3)_2$ uniquely deposited only into the semi-transparent green characteristic of the hydrated $Ni(OH)_2$ state and the Ni^0 state was not detected coulometrically for < 1.25 mA/cm^2 deposition current densities [12].

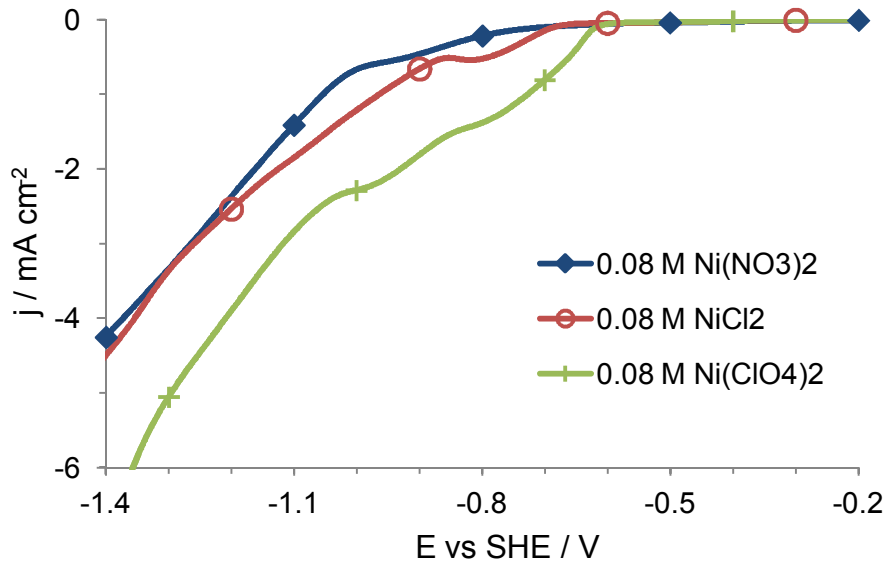

Figure 1. Linear sweep voltammograms at -10 mV/s on HOPG for 0.08 M $Ni(NO_3)_2$, $NiCl_2$, and $Ni(ClO_4)_2$ electrolytes.

The most active NiOOH materials could only be generated at low concentrations (0.08 M $Ni(NO_3)_2$) and relatively high current densities (-1 mA/cm^2). A high reactant (Ni^{2+}) concentrations and low deposition current density would instead be preferable for depositing active material inside a porous current collector. These conditions would be preferable because they will minimize reactant concentration gradients within the porous current collector as the Ni^{2+} is consumed during deposition so

that the active material is evenly distributed throughout the current collector. Low current densities alternatively generate low interfacial OH^- concentrations and were expected to be less effective at precipitating $Ni(OH)_2$ at low Ni^{2+} concentrations according to equilibrium of (4). The most efficient deposition current efficiencies and activities occurred around -1 mA/cm^2 for 0.08 M $Ni(NO_3)_2$ solutions (Figure 2). The dramatic decrease in electrodeposition current efficiency and/or activity for current densities > 1.1 mA/cm^2 corresponded with the detection of both Ni^0 and anhydrous NiO according to the charge initiation at -0.3 V vs SHE as well as the transition from green to dark colored deposits. This optimal deposition current density was exceptionally high when evaluated by equation (9), where j is the diffusion limited current density in A/cm^2, $[Ni^{2+}]$ is the molar concentration, γ is the Ni^{2+}'s activity coefficient, $D_{½Ni2+}$ is the diffusion coefficient of 0.661 x 10^{-5} cm^2/s at infinite dilution and 25 °C , and ς is the diffusion layer thickness [17].

$$j = \frac{nFD_{1/2Ni2+}\gamma[Ni^{2+}]}{1000 \cdot \varsigma} \qquad (9)$$

The divalent Ni^{2+} ion's activity coefficient is low at 0.3 for 0.08 M $Ni(NO_3)_2$, which corresponds to a Ni^{2+} diffusion layer thickness of 280 µm at -1 mA/cm^2. Significant mass transport complications would be expected for the deposition of active material into 1 µm sized pores when the Ni^{2+} diffusion layer thickness is over 2 orders of magnitude larger for the narrow range of deposition current densities required for optimal activity. The mass of deposited Ni^{2+} ion was determined through ICP-MS and an ideal current efficiency of 2 e^- per Ni atom deposited occurred at 1.0 mA/cm^2 (Figure 3). The optimal electrodeposition current density of -1 mA/cm^2 corresponded to a condition where the overpotential decreased by approximately 100 mV over 100 – 150 s and then reached a steady state condition as the potential became constant for ≥ 30 min. Significant losses in electrodeposition current efficiency and/or activity occurred when the electrodeposition technique was changed from constant current to constant

potential despite the application of the same current/potential ranges, which also indicate the mass transfer rate-dependence of the electrodeposition mechanism expected from reactions (4) – (6).

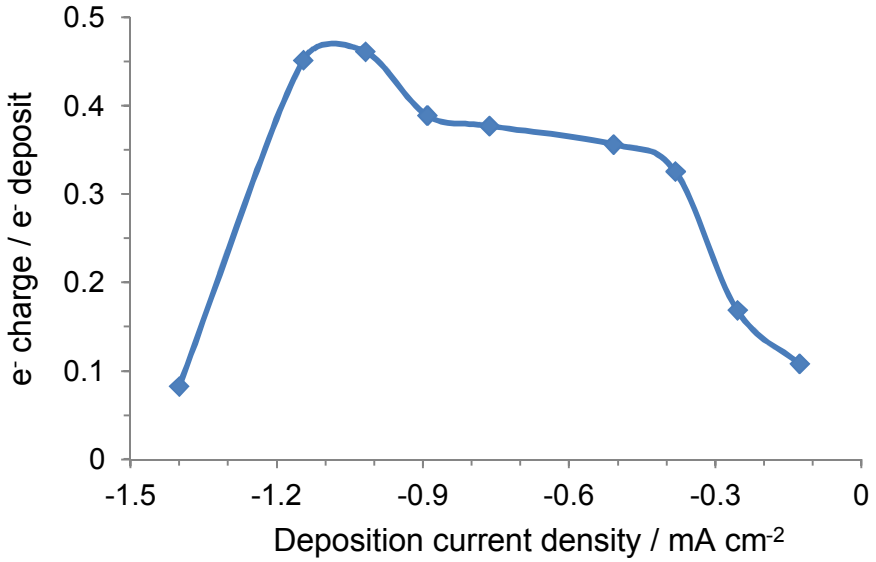

Figure 2. Deposition activity efficiency. The fraction of e^- charge storable in a $Ni(OH)_2$ deposit at a 2C rate per the number of e^- passed to deposit the $Ni(OH)_2$ onto HOPG as a function of the deposition current density for a 0.08 M $Ni(NO_3)_2$ solution.

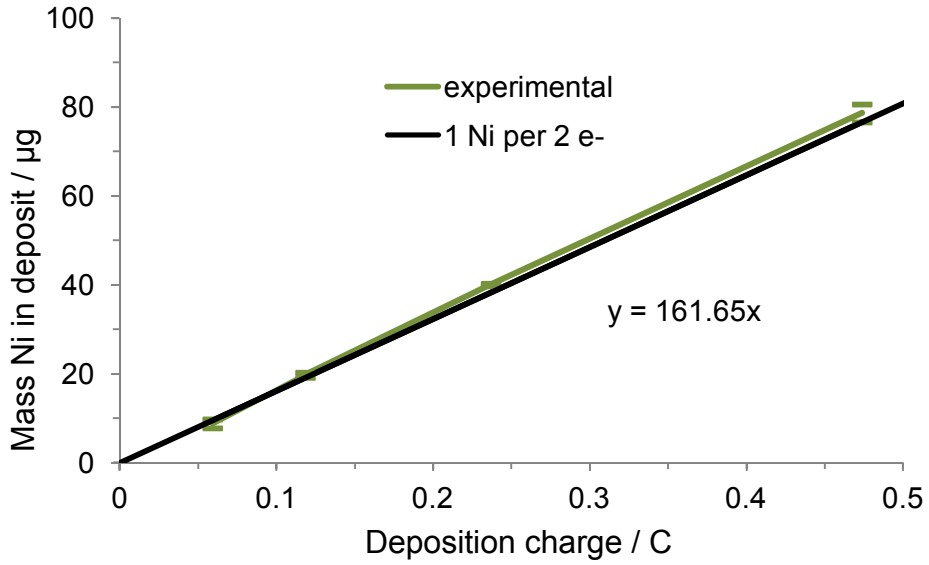

Figure 3. Deposition current efficiency. The mass of Ni deposited as $Ni(OH)_2$ per coulomb of deposition charge with a -1.0 mA/cm^2 deposition current density from 0.08 M $Ni(NO_3)_2$.

The morphology of the deposited $Ni(OH)_2$ was not ideal for electrodeposition into a porous structure sub-micron pores. In addition to the narrow current density range required for optimal activity, the cathodic electrodeposition formed porous clumps under constant current. The 300 mC charge passed during deposition at -1 mA/cm^2 was expected to form a film 0.22 µm thick, assuming the density of 4.15 g/cm^3, because the electrodeposition current efficiency was 100 %. The $Ni(OH)_2$ instead formed clumps with heights of about 1.5 µm. The morphology of Figure 4A indicates that the density of the $Ni(OH)_2$ may be approximately half of the expected 4.15 g/cm^3. A non-dense deposit is necessary if OH^- generated on the current collector interface needs to diffuse through the insulating $Ni(OH)_2$ deposit to precipitate reactant Ni^{2+} according to (5) [10]. A non-dense and high surface area deposit from cathodic electrodeposition was expected due to the resulting material's proficiency for supercapacitor applications [18-21]. Switching to a 0.3 s pulse at -1.0 mA/cm^2 and 2.1 s pauses resulted in a more evenly distributed film with a significantly lower electrodeposition current efficiency and/or activity (Figure 4B). 0.3 % Ni^0 was detected in the deposit from the pulse method. Ni^0 may deposit upon HOPG at the initiation of current, where subsequent oxidation to $Ni(OH)_2$ by NO_3^- established nucleation sites for further chemical precipitation through (4).

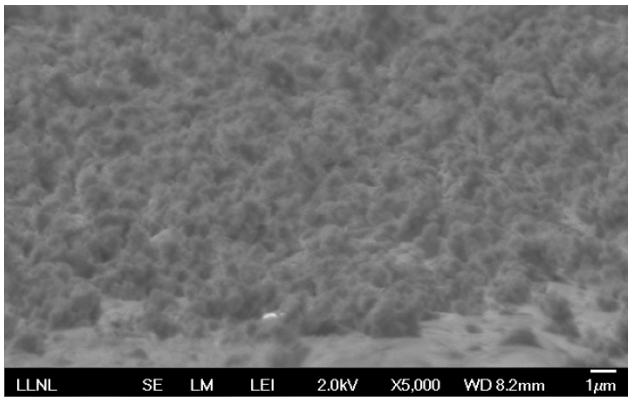

Figure 4A. $Ni(OH)_2$ deposited with 300 mC at -1 mA/cm^2.

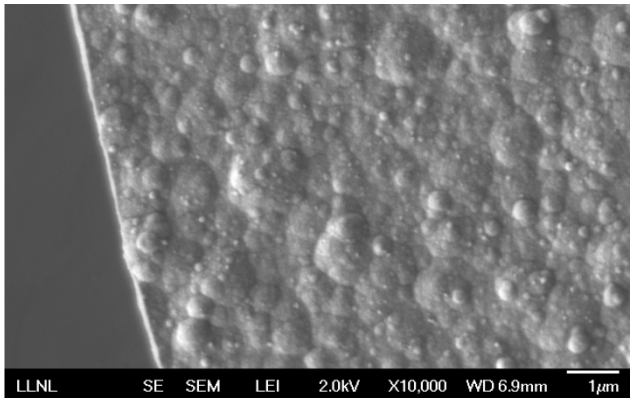

Figure 4B. $Ni(OH)_2$ deposited with 300 mC at -1 mA/cm^2 in 0.3 s pulses and 2.1 s pauses.

The $Ni(OH)_2$ deposited at -1.0 mA/ became fully charged when oxidized by 1.79 +/- 0.02 e^- per Ni ion and could subsequently deliver 1.58 +/- 0.02 e^- per Ni ion. The maximum charge was experimentally limited by oxygen evolution from water and was slightly larger than the commonly reported maximum value of 1.7 +/- 0.1 e^- [7]. The ability to discharge 1.58 e^- per Ni was much larger than the rare 1 e^- per Ni and the more typical 0.4 e^- [6, 22]. The $Ni(OH)_2$ needed to be initially charged at a rate ≥ 20 C (Figure 5). This extremely fast initial charge required an overpotential of 80 – 100 mV and may indicate that active material needs to be oxidized quickly enough that the transport of H^+ product from bulk $Ni(OH)_2$ to the electrolyte was rate-limiting. The initial discharge rate had to be ≤ 2C, where slower discharge rates did not release more charge. Assuming a molecular weight of 92.7 g/mol, the

deposit needed to be ≤ 0.15 mg of $Ni(OH)_2$ distributed over 1 cm^2 of flat HOPG surface or ≤ 0.22 um thick assuming a density of 4.15 g/cm^3.

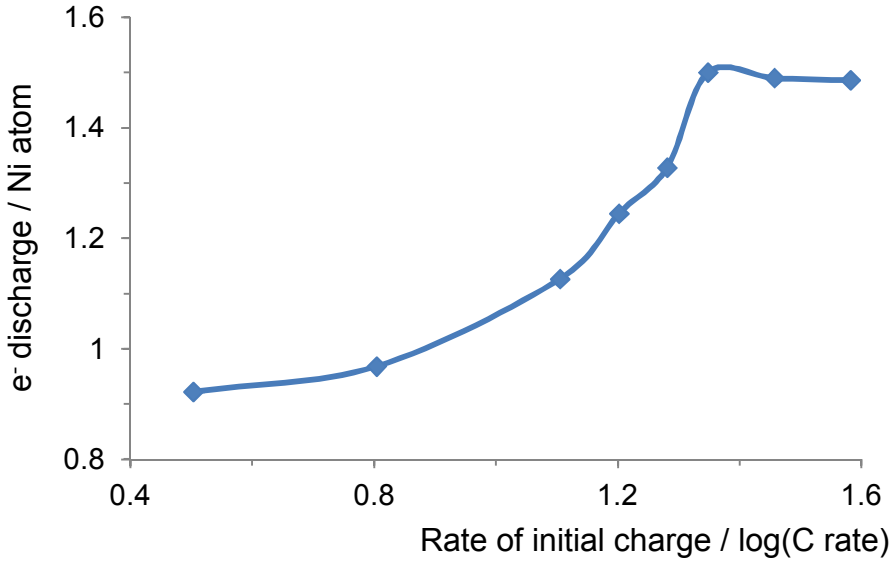

Figure 5. The dependence of the discharge activity at 2 C upon the initial charge C rate for a 0.25 mg/cm^2 loading deposited from 0.08 M $Ni(NO_3)_2$ at -1 mA/cm^2.

The cathodic deposition of $Ni(OH)_2$ onto HOPG and its uniquely large activity offered a novel opportunity to thermodynamically explore the nickel oxide's charge and discharge mechanisms in what may be the maximum activity. Precipitated $Ni(OH)_2$ is typically characterized as a more ordered β-$Ni(OH)_2$ or a more disordered and hydrated active α- $Ni(OH)_2$ [10, 11, 23-25]. The more active but less stable α- $Ni(OH)_2$ can transfer almost 2 e^- per active Ni atom where only one phase change occurs as changes in only the one, broad spectroscopic peak were observed *in situ* [7-9]. Corrigan argued that this indicated a homogeneous distribution of valence states, such as Ni^{2+}, Ni^{3+}, and Ni^{4+}, and that discreet states do not exist [7, 9]. Several issues arise with Corrigan's mechanism (3) and conclusions in the context of a thermodynamic analysis. A homogenous distribution of valence states would produce symmetrical charge and discharge curves. However, it is known experimentally that there is substantial asymmetry or hysteresis between charge and discharge curves that occurs even when the rates

approach steady state conditions [5, 26]. The product of (3) doesn't actually correspond with the known oxidation states indicated in Table 2, it can not be corroborated by known free enthalpies of formation, and an evaluation of the pH and potential-dependence of the charge/discharge curves could not indicate support of that mechanism. Corrigan also did not actually detect Ni^{4+} spectroscopically [7, 9]. The Ni^{4+} oxidation state in (13) should additionally be considered kinetically unlikely because of the large number of H_2O species which would require transport through the solid bulk material as well as a corresponding large volume change [12]. Exchange between (10) – (12) should be relatively facile because they only require the transport of the small H^+ within the bulk phase of "NiOOH".

Table 2. Equations (10a) – (14a): Known nickel and oxygen redox reactions [12].

$$Ni_3O_4(H_2O)_2 + 2\cdot H^+ + 2\cdot e^- \leftrightarrow 3\cdot NiO(H_2O) \quad (10)$$
$$E_0(10a) = 0.897 - 0.05916\cdot pH$$
$$E_0(10b) = 0.837 - 0.05916\cdot pH$$
$$Ni_2O_3(H_2O) + 2\cdot H^+ + 2\cdot e^- \leftrightarrow 2\cdot NiO(H_2O) \quad (11)$$
$$E_0(11a) = 1.032 - 0.05916\cdot pH$$
$$E_0(11b) = 0.912 - 0.05916\cdot pH$$
$$3\cdot Ni_2O_3(H_2O) + 2\cdot H^+ + 2\cdot e^- \leftrightarrow 2\cdot Ni_3O_4(H_2O)_2 \quad (12)$$
$$E_0(12a) = 1.305 - 0.05916\cdot pH$$
$$E_0(12b) = 1.184 - 0.05916\cdot pH$$
$$2\cdot NiO_2(H_2O)_2 + 2\cdot H^+ + 2\cdot e^- \leftrightarrow Ni_2O_3(H_2O) + 4\cdot H_2O \quad (13)$$
$$E_0(13) = 1.434 - 0.05916\cdot pH$$
$$\tfrac{1}{2}O_2 + 2\cdot H^+ + 2\cdot e^- \leftrightarrow H_2O \quad (14)$$
$$E_0(14a) = 1.228 - 0.05916\cdot pH$$
$$E_0(14b) = 1.288 - 0.05916\cdot pH$$

The problem with using equations (10a) – (14a) in an aqueous environment is how to treat the hydrating H_2O indicated in Pourbaix's enthalpy of formation. The thermodynamic difference between liquid and solid water at 25 °C is that $H_2O_{(l)}$ has a standard entropy, ΔS_m^0, of 69.9 J/K/mol while $H_2O_{(s)}$ has 38.0 J/K/mol [27]. The $NiO(H_2O)$ is notably the only oxidation state which dehydrates and it is

thermodynamically more favorable for the oxidation state to dehydrate prior to oxidation. Are all of the hydrating water species the same for all of the different oxidation states and should they be treated with liquid phase thermodynamic values? Pourbaix considered all of the hydrating H_2O to have entropies equivalent to that of $H_2O_{(l)}$ and this affected the redox values reported. A comparison between NiO and $NiO(H_2O)$ values indicates that the hydrating water can have a more liquid-like ΔS_m^0 as high as 68.6 J/K/mol or a lower value of 65.5 J/K/mol, which may correspond the α- and β- phases, respectively [12, 28]. It will be assumed here that the water associated with each Ni^{2+}, $H_2O_{(l')}$, has the liquid-like entropy while the water associated with Ni^{3+}, $H_2O_{(s)}$, has the solid phase entropy so that the states considered are $NiO(H_2O_{(l')})$, $Ni_3O_4(H_2O_{(s)})(H_2O_{(l')})$ and $Ni_2O_3(H_2O_{(s)})$. The distinction in hydrating water species means that the redox potentials need to be recalculated as the beta form in Table 2. The oxidation of $H_2O_{(s)}$ hydrating the metal oxide is 60 mV less favorable than $H_2O_{(l)}$.

A "NiOOH" mechanism consistent with the experimental data can be constructed using the beta equilibria of Table 2. The key to modeling the "NiOOH" mechanism with distinct local domains is the known hypothesis that oxygen undergoes redox chemistry in addition to the Ni ions, which is necessary when almost 2 e^- per Ni ion are storable while Ni^{4+} isn't spectroscopically detectable [7, 9]. The active material's charge occurred above the oxygen evolution equilibrium (14), where a water molecule can be oxidized into an oxygen atom, $½O_2$. The mechanism is centered around the Ni^{2+}, $Ni^{2.67+}$, and Ni^{3+}, valence states, where the hydrating $H_2O_{(s)}$ are oxidized into $½O_2$ plus 2 H^+ and 2 e^-. The disproportionation and amphoterization involved with the local domain state interactions governed by (10) – (14) can cause differentiation in the charge and discharge mechanisms so that there is asymmetry or hysteresis between the charge and discharge curves. The -120 mV/pH dependence of the charge curve asymptotes and the -60 mV/pH dependence of the discharge curve asymptotes at steady state conditions indicated asymmetry or hysteresis and that the charge and discharge mechanisms were not the reverse of each other. The asymptotes of charge and discharge curves of Figure 6 are illustrated in Figure 7 and should

correspond to rational equilibria in an approximately ideal system. The slight deviations of the experimentally determined asymptotes in kinetic curves from the theoretical equilibria at the highest KOH concentrations was likely due to the significant deviation of the solvent water's activity or osmotic coefficients from the ideal condition assumed in the thermodynamic calculations [12, 29].

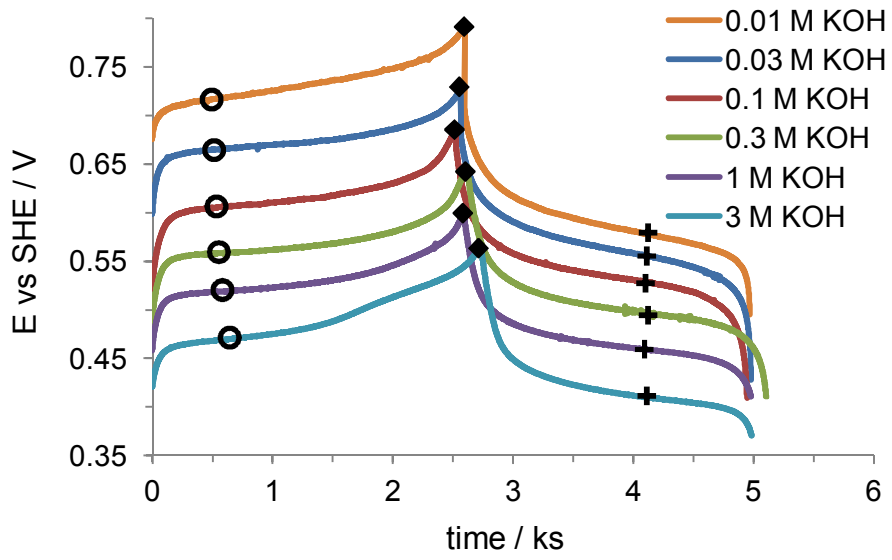

Figure 6. The potential dependence of the 2nd charge/discharge curves with respect to KOH concentration for 0.25 mg/cm^2 loadings deposited from 0.08 M $Ni(NO_3)^2$ at -1 mA/cm^2. The indicated asymptotes are evaluated in Figure 7.

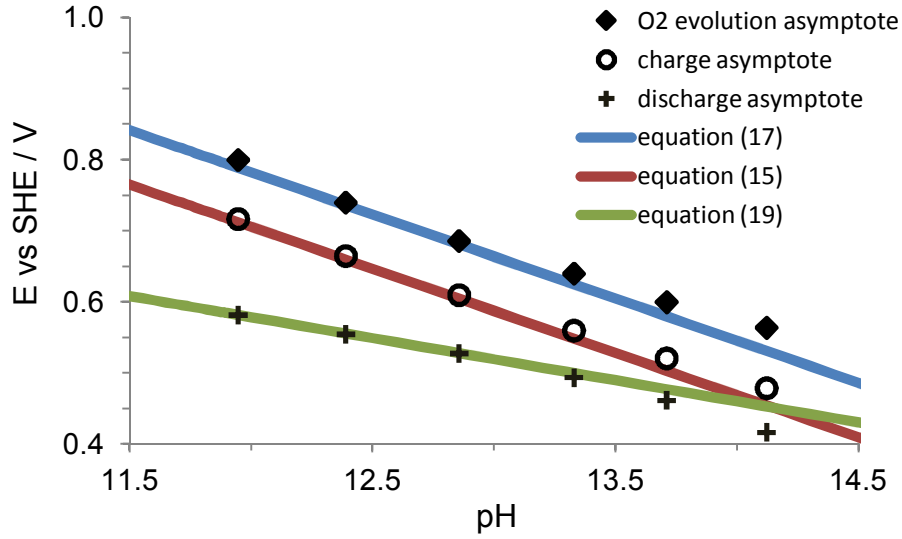

Figure 7. The correlation of experimental kinetic asymptotes of Figure 6 with electrochemical equilibria.

The redox activity of oxygen through (14b) must involve the $Ni_3O_4(H_2O)_2$ oxidation state because the oxidation of $Ni(OH)_2$ through (10b) or (11b) is thermodynamically more favorable than (14b). The application of the overcharge required to oxidize the initial $Ni(OH)_2$ deposit at a rate of 30 C may have helped select for reaction (15) over (10b) or (11b). The thermodynamics indicate that $½O_2$ is stabilized in the $H_2O_{(s)}$ position so that the product is $Ni_3O_4(½O_2)(H_2O_{(l')})$ and the charging asymptote correlated with (15) (Figure 7). The potential during charge surpasses the disproportionation reaction of (16) so that $Ni_3O_4(H_2O_{(s)})(H_2O_{(l')})$ can spontaneously transition into separate $NiO(H_2O_{(l')})$ and $Ni_2O_3(H_2O_{(s)})$ states. The degeneracy of (16) provides a means for all of the Ni ion in $Ni_3O_4(½O_2)(H_2O_{(l')})$ to reach the $Ni_2O_3(½O_2)$ state as the latter becomes stable according to (17). The "NiOOH" therefore oxidizes through (18) at the potential of (17), which corresponded with the experimental charging curve asymptotes caused by oxygen evolution. The proposed fully charged state is absent of both $H_2O_{(l')}$ and $H_2O_{(s)}$ and in accordance with Corrigan's inability to detect OH^- interactions with Ni ions in the fully charged condition. The intermediate state of $Ni_3O_4(½O_2)(H_2O_{(l)})$ has released 1.67 e^- per Ni ion, the ideal charged state of $Ni_2O_3(½O_2)$ has released 2.00 e^- per Ni ion, and the equilibrium condition between the two states corresponded to the experimental limit of oxygen evolution where the "NiOOH" was oxidized by 1.84 +/- 0.02 e^- per Ni ion.

Table 3. Equations (15) – (): relevant charge and discharge mechanisms.

$$3\cdot NiO\left(H_2O_{(l')}\right)\leftrightarrow Ni_3O_4\left(\tfrac{1}{2}O_2\right)\left(H_2O_{(l')}\right)+4\cdot H^+ +4\cdot e^- \quad (15)$$

$$E_0(15)=1.288+0.837-2\cdot 0.05916\cdot pH$$

$$Ni_3O_4\left(H_2O_{(s)}\right)\left(H_2O_{(l')}\right)\leftrightarrow NiO\left(H_2O_{(l')}\right)+Ni_2O_3\left(H_2O_{(s)}\right) \quad (16)$$

$$E_0(16)=0.837+1.184-2\cdot 0.05916\cdot pH$$

$$2\cdot NiO\left(H_2O_{(l')}\right)\leftrightarrow Ni_2O_3\left(\tfrac{1}{2}O_2\right)+2\cdot H^+ +2\cdot e^- \quad (17)$$

$$E_0(17) = 1.288 + 0.912 - 2 \cdot 0.05916 \cdot pH$$

$$2 \cdot Ni_3O_4(\tfrac{1}{2}O_2)(H_2O_{(l')}) \leftrightarrow 3 \cdot Ni_2O_3(\tfrac{1}{2}O_2) + 2 \cdot H^+ + 2 \cdot e^- \quad (18)$$

$$Ni_2O_3(\tfrac{1}{2}O_2) \leftrightarrow 2 \cdot NiO(\tfrac{1}{2}O_2) \quad (19)$$

$$NiO(\tfrac{1}{2}O_2) + 2 \cdot H^+ + 2 \cdot e^- \leftrightarrow +NiO(H_2O_{(s)}) \quad (20)$$

$$E_0(18) = 1.288 - 0.05916 \cdot pH$$

$$3 \cdot NiO(H_2O) + 2 \cdot F^- \leftrightarrow Ni_3O_3(H_2O_{(s)})(H_2O_{(l')})F_2 + H_2O + 2 \cdot e^- \quad (21)$$

$$2 \cdot Ni_3O_3(H_2O_{(s)})(H_2O_{(l')})F_2 \leftrightarrow 3 \cdot Ni_2O_3(\tfrac{1}{2}O_2) + 4 \cdot H^+ + 4 \cdot e^- + 4 \cdot F^- \quad (22)$$

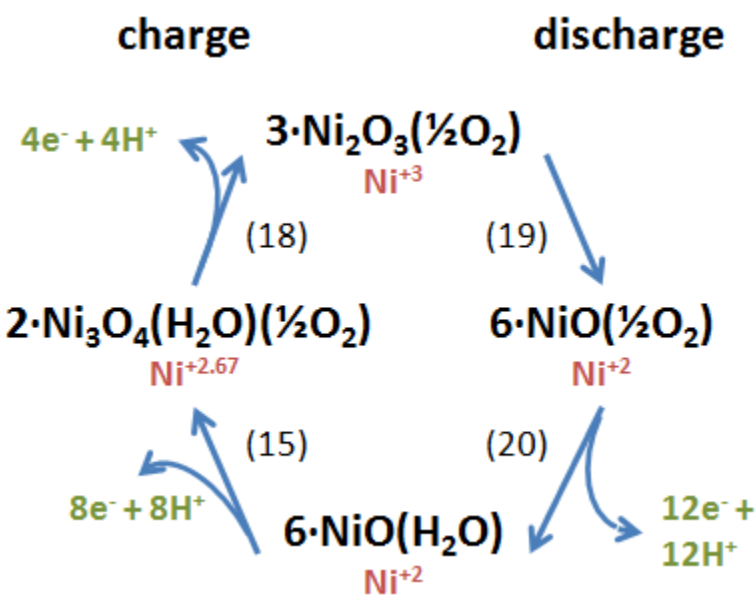

Figure 8. The ideal "NiOOH" active cycle.

The proposed charging process indicates that the fully charged condition was composed of predominantly $Ni_2O_3(\tfrac{1}{2}O_2)$ plus a fraction of Ni^{3+} whose $\tfrac{1}{2}O_2$ is absent due to oxygen evolution. The Ni^{3+} constitutes 20 – 22 % of the nickel in the charged condition and was inert during the discharge process because the "NiOOH" finished discharging before approaching the potential of (12b). The "NiOOH" has been commonly assumed to discharge though (12) because of the similarity of the inaccurate potential of (12a) with the experimental discharge asymptote. The ability to only discharge a maximum 0.33 of the stored 1.58 e^- per Ni ion in combination with an absence of discharge through the distinct potentials

of (10a/b), (11a/b), or (12b) means that the discharge of the Ni^{3+} unassociated with ½O_2 to $Ni^{2.67+}$ cannot be a predominant mechanism if it's active at all. Discharge through (12b) only appeared after significant (> 50 %) deactivation of the "NiOOH" through repetitive cycling. The absence of any nickel discharge mechanisms in addition to the discharge of 1.58 e^- per Ni ion meant that all of the Ni_2O_3(½O_2) must relax into NiO(½O_2) according to (19) and all of the discharge must occur through (14b)/(20). The 7 – 9 % charge loss due to the inability to completely charge the "NiOOH" because of oxygen evolution plus a 4 – 5 % charge loss due to instability with cycling causes the "NiOOH" to only be able to discharge by 1.58 +/- 0.02 e^- per Ni ion to an average Ni valence of +2.25 +/- 0.02. The potential overlap of the initial charging mechanism of (15) with the discharging mechanism of (20) at pH 14.1 caused an oxygen evolution short circuit which prohibited charging the "NiOOH" without the overpotential of a fast charging C rate of > 20.

The $H_2O_{(l')}$ and $H_2O_{(s)}$ was experimentally distinguishable because of the exchange of $H_2O_{(l')}$ with the aqueous solvent. Water's self-diffusion is exceptionally fast because it involves the dissociation into $H^+ + OH^-$ in an intermediate state [30, 31]. This solvent exchange mechanism can be inhibited in a condition when an F^- ion (133 pm) can thermodynamically outcompete OH^- (133 pm). Solution phase calculations supported by experimental results indicated that the electronegative F^- is competitive with OH^- for Ni^{2+} in a 1 M KF : 0.01 M KOH solution [32]. The inhibition by F^- caused oxidation by 0.67 e^- per Ni ion to the $Ni_3O_3(H_2O_{(s)})(H_2O_{(l')})F_2$ according to (21) and the coulometric charge indicated in Figure 10. Elemental analysis after the first charge step at the point marked by ⍰ indicated that there was 0.59 of the 0.67 F per Ni predicted in the product of (21). The asymptote of this initial charge mechanism was approximately +120 mV greater (12b) as expected from the thermodynamics of the 100X difference in concentrations indicated by the solution phase equilibria calculations. The subsequent oxidation of $Ni_3O_3(H_2O_{(s)})(H_2O_{(l')})F_2$ to Ni_2O_3(½O_2) by (22) was limited halfway through the reaction by oxygen evolution just like (18) was limited halfway by oxygen evolution. The limitation of charging halfway

through (22) correlated with the second step where the "NiOOH" was oxidized by another 0.67 e^- per Ni ion (Figure 10) as well as 0.31 of the expected 0.33 F per Ni measured at the point marked by □. The potential-dependence demonstrated by the effects of KF in the electrolyte suggests that the number of hydrating H_2O which can exchange with the solution phase could change with activity, cycling, or exchange with KOH and may explain the potential shifts which occur with aging [5].

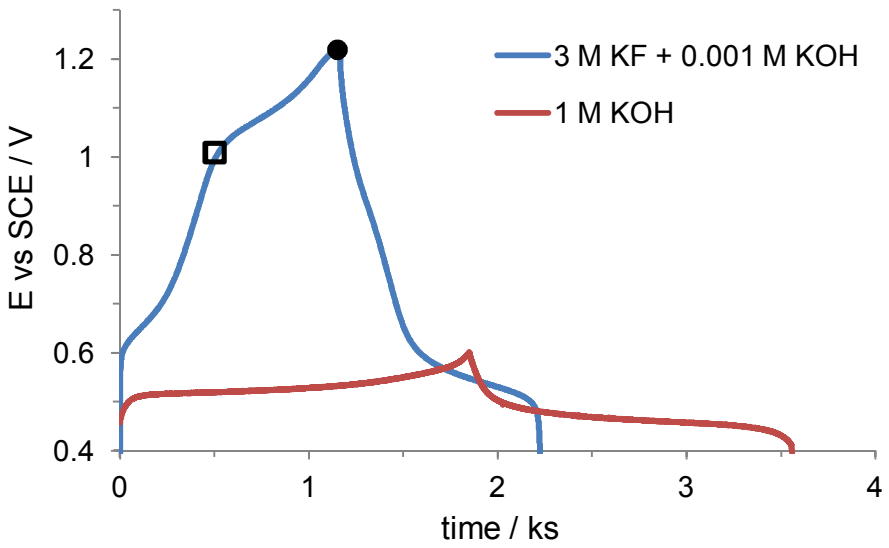

Figure 10. The partial inhibition of the charging mechanism with F- for 0.25 mg/cm^2 loadings deposited from 0.08 M $Ni(NO_3)^2$ at -1 mA/cm^2. The symbols □ and □ indicate where the "NiOOH" charged in KF was sampled for elemental analysis.

The highly active nickel material was unstable throughout repeated charge and discharge cycles (Figure 11). The film thickness, charge and discharge rates, depth of discharge, overcharge, electrolyte KOH concentration, or the addition of LiOH to the electrolyte did not improve the stability significantly enough (data not shown) to be useful in practical rechargeable battery applications as charge storage capability degenerated with a ~ 5 % loss with each successive charge or discharge. Despite the new

insight into the charge/discharge mechanism, it is not yet clear whether highly active "NiOOH" materials can have competitive stabilities or if the deactivation by changes in the hydrated states are unavoidable.

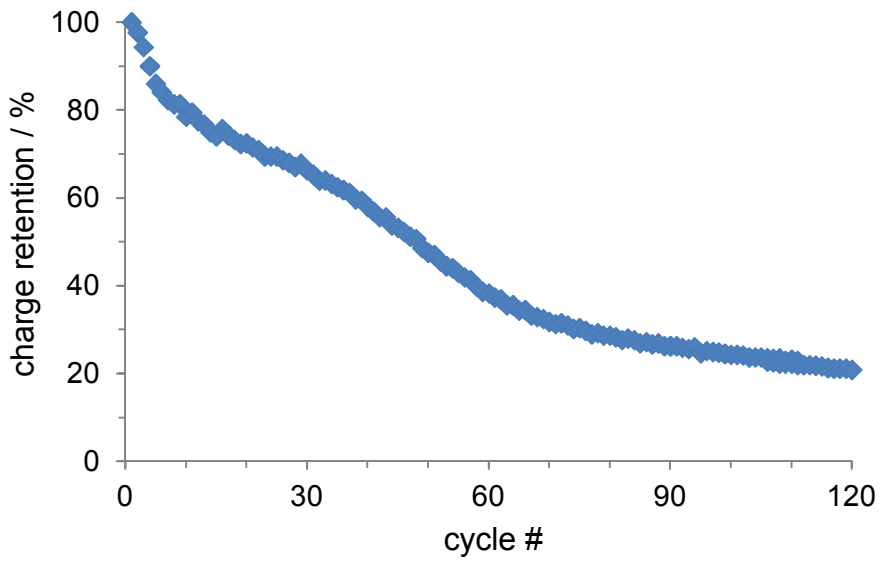

Figure 11. Cycle stability at a 2 C rate in 1 M KOH for a 0.25 mg/cm^2 loading deposited from 0.08 M $Ni(NO_3)^2$ at -1 mA/cm^2.

Conclusion

Graphite caused the nitrate reduction reaction, the hydrogen evolution reaction, and the metallic Ni deposition reactions to all initiate at approximately the same potential. The interactions of multiple electrochemical reactions during the cathodic electrodeposition of $Ni(OH)^2$ onto graphite attained an ideal electrodeposition current efficiency at an exceptionally high current density. Highly active "NiOOH" materials of modest thicknesses were generated which could be initially oxidized up to store up to 1.84 e^- per Ni ion and could subsequently store a charge of 1.58 e^- per Ni ion. The approximately ideal charge capacity of the "NiOOH" facilitated a thermodynamic analysis through which the specific charge and discharge mechanisms could be resolved from the enthalpies of formation for known states. The mechanisms and were in accordance with the pH, potential dependence, charge

quantities, hysteresis, and fluoride ion partial inhibition of the charge and discharge curves as well as Corrigan's spectroscopic results. The valence of the Ni ion changes between 2+ and 3+ during the charge and discharge processes however the redox activity of oxygen allows the charge storage of a second e^- per Ni ion. Poor morphology and stability with cycling however would limit practical application.

Prepared by LLNL under Contract DE-AC52-07NA27344.

1. Reddy, T. and D. Linden, *Linden's Handbook of Batteries*. 2010: McGraw-Hill.
2. Baumann, T.F. and J.H. Satcher Jr, *Template-directed synthesis of periodic macroporous organic and carbon aerogels.* Journal of Non-Crystalline Solids, 2004. **350**(0): p. 120-125.
3. Biener, J., et al., *Advanced carbon aerogels for energy applications.* Energy & Environmental Science, 2011. **4**(3).
4. Rolison, D.R., et al., *Multifunctional 3D nanoarchitectures for energy storage and conversion.* Chemical Society Reviews, 2009. **38**(1).
5. Zimmerman, A.H., *Nickel-hydrogen batteries: principles and practice*. 2009: Aerospace Press.
6. Zhang, H.G., X.D. Yu, and P.V. Braun, *Three-dimensional bicontinuous ultrafast-charge and -discharge bulk battery electrodes.* Nature Nanotechnology, 2011. **6**(5): p. 277-281.
7. Corrigan, D.A. and S.L. Knight, *Electrochemical and Spectroscopic Evidence on the Participation of Quadrivalent Nickel in the Nickel Hydroxide Redox Reaction.* Journal of The Electrochemical Society, 1989. **136**(3): p. 613-619.
8. Carpenter, M.K. and D.A. Corrigan, *Photoelectrochemistry of Nickel Hydroxide Thin Films.* Journal of The Electrochemical Society, 1989. **136**(4): p. 1022-1026.
9. Desilvestro, J., D.A. Corrigan, and M.J. Weaver, *Characterization of Redox States of Nickel Hydroxide Film Electrodes by In Situ Surface Raman Spectroscopy.* Journal of The Electrochemical Society, 1988. **135**(4): p. 885-892.
10. Wohlfahrt-Mehrens, M., et al., *The mechanism of electrodeposition and operation of Ni(OH)2 layers.* Solid State Ionics, 1996. **86–88, Part 2**(0): p. 841-847.
11. Jayashree, R.S. and P.V. Kamath, *Nickel hydroxide electrodeposition from nickel nitrate solutions: mechanistic studies.* Journal of Power Sources, 2001. **93**(1–2): p. 273-278.
12. Pourbaix, M., *Atlas of electrochemical equilibria in aqueous solutions*. 1974: National Association of Corrosion Engineers.
13. Bouzek, K., et al., *Electrochemical reduction of nitrate in weakly alkaline solutions.* Journal of Applied Electrochemistry, 2001. **31**(11): p. 1185-1193.
14. Taylor, C.D., et al., *First principles reaction modeling of the electrochemical interface: Consideration and calculation of a tunable surface potential from atomic and electronic structure.* Physical Review B, 2006. **73**(16): p. 165402.
15. Sonavane, A.C., et al., *Efficient electrochromic nickel oxide thin films by electrodeposition.* Journal of Alloys and Compounds, 2010. **489**(2): p. 667-673.

16. Nam, K.-W., et al., *Synthesis and Electrochemical Investigations of Ni[sub 1 - x]O Thin Films and Ni[sub 1 - x]O on Three-Dimensional Carbon Substrates for Electrochemical Capacitors.* Journal of The Electrochemical Society, 2005. **152**(11): p. A2123-A2129.
17. Bard, A.J. and L.R. Faulkner, *Electrochemical methods: fundamentals and applications*. 2001: Wiley.
18. Kalu, E.E., et al., *Cyclic voltammetric studies of the effects of time and temperature on the capacitance of electrochemically deposited nickel hydroxide.* Journal of Power Sources, 2001. **92**(1–2): p. 163-167.
19. Zhao, D.-D., et al., *Preparation of hexagonal nanoporous nickel hydroxide film and its application for electrochemical capacitor.* Electrochemistry Communications, 2007. **9**(5): p. 869-874.
20. Nam, K.-W. and K.-B. Kim, *A Study of the Preparation of NiO[sub x] Electrode via Electrochemical Route for Supercapacitor Applications and Their Charge Storage Mechanism.* Journal of The Electrochemical Society, 2002. **149**(3): p. A346-A354.
21. Zhang, X., et al., *Synthesis of porous NiO nanocrystals with controllable surface area and their application as supercapacitor electrodes.* Nano Research, 2010. **3**(9): p. 643-652.
22. Wang, H., et al., *Ni(OH)2 Nanoplates Grown on Graphene as Advanced Electrochemical Pseudocapacitor Materials.* Journal of the American Chemical Society, 2010. **132**(21): p. 7472-7477.
23. Oliva, P., et al., *Review of the structure and the electrochemistry of nickel hydroxides and oxy-hydroxides.* Journal of Power Sources, 1982. **8**(2): p. 229-255.
24. Nazri, G., D.A. Corrigan, and S.P. Maheswari, *Angle-resolved infrared spectroelectrochemistry. 1. An in situ study of thin-film nickel oxide electrodes.* Langmuir, 1989. **5**(1): p. 17-22.
25. Pandya, K.I., et al., *Extended x-ray absorption fine structure investigations of nickel hydroxides.* The Journal of Physical Chemistry, 1990. **94**(1): p. 21-26.
26. Srinivasan, V., J.W. Weidner, and J. Newman, *Hysteresis during cycling of nickel hydroxide active material.* Journal of The Electrochemical Society, 2001. **148**(9): p. A969-A980.
27. Atkins, P. and J.D. Paula, *Physical Chemistry*. 2009: W. H. Freeman and Co.
28. Haynes, W.M., *CRC handbook of chemistry and physics : a ready-reference book of chemical and physical data*. 2011, Boca Raton, FL.: CRC Press.
29. Hamer, W.J. and Y.-C. Wu, *Osmotic Coefficients and Mean Activity Coefficients of Uni-univalent Electrolytes in Water at 25[degree]C.* Journal of Physical and Chemical Reference Data, 1972. **1**(4): p. 1047-1100.
30. Eigen, M., *Methods for investigation of ionic reactions in aqueous solutions with half-times as short as 10-9 sec. Application to neutralization and hydrolysis reactions.* Discussions of the Faraday Society, 1954. **17**.
31. Dippel, T. and K.D. Kreuer, *Proton transport mechanism in concentrated aqueous solutions and solid hydrates of acids.* Solid State Ionics, 1991. **46**(1–2): p. 3-9.
32. Engineering, D.o.L.a.W.R., *Visual MINTEQ 2.54*, in http://www.lwr.kth.se/English/OurSoftware/vminteq/, K.R.I.o. Technology, Editor. 2010: Stockholme.